Preprint Title KPFM work function characterization of ongoing reduction and oxidation of transition metal oxide crystals on examples of $SrTiO_3$ and TiO nanowires

Authors Dominik Wrana, Karol Cieślik, Wojciech Bełza, Christian Rodenbücher, Krzysztof Szot and Franciszek Krok

Article Type Full Research Paper

ORCID® iDs Dominik Wrana - https://orcid.org/0000-0002-8239-0043; Karol Cieślik - https://orcid.org/0000-0002-1069-1840

KPFM work function characterization of ongoing reduction and oxidation of transition metal oxide crystals on examples of $SrTiO_3$ and TiO nanowires

D. Wrana[1,*], K. Cieślik[1], W. Belza[1], C. Rodenbücher[2], K. Szot[3,4] and F. Krok[1]

[1]*Marian Smoluchowski Institute of Physics, Jagiellonian University, Lojasiewicza 11, 30-348 Krakow, Poland.*
**dominik wrana – dominik.wrana@uj.edu.pl*
[2]*Institute of Energy and Climate Research (IEK-3), Forschungszentrum Jülich GmbH, 52425 Jülich, Germany*
[3]*Peter Grünberg Institute (PGI-7), Forschungszentrum Jülich GmbH , 52425 Jülich, Germany.*
[4]*August Chelkowski Institute of Physics, University of Silesia, 40–007 Katowice, Poland*

Abstract

Controlling the work function of transition metal oxides is of key importance towards future energy production and storage. As majority of applications comprise the use of heterostructures, the most suitable experimental technique is Kelvin Probe Force Microscopy, providing excellent energetic and lateral resolution. In this paper we demonstrate the possibility of the precise work function characterization using the example of artificially formed crystalline titanium monoxide TiO nanowires on strontium titanate $SrTiO_3$ surfaces providing a sharp atomic interface. The measured value of 3.31(21) eV is the first experimental work function evidence for a cubic TiO phase, being additionally subjected to significant variations among different crystallographic facets. Despite the remarkable height of the formed TiO nanowires, FM-KPFM proved to be able to achieve high lateral resolution of 15 nm, which is close to the topographical limits. In this study we show also the unique possibility of obtaining conductivity and work function maps on the same area, by combining contact and non-contact atomic force microscopy. As most of real applications require ambient operating conditions, we have additionally checked the impact of air venting on the work function of the $TiO/SrTiO_3(100)$ heterostructure, proving the surface re-oxidation occurs and results in work function increases of 0.9 eV and 0.6 eV for $SrTiO_3$ and TiO, respectively. In addition, the influence of physisorbed species was estimated to contribute 0.4 eV and 0.2 eV to the work function of both structures. The presented method of the KPFM (and LC-AFM) employment for the work function characterization of transition metal oxides may help to understand the reduction and oxidation impact on electronic properties, which is of high importance towards the development of effective sensing and catalytic devices.

Keywords

Work function; transition metal oxides; FM-KPFM, Kelvin Probe Force Microscopy; reduction and oxidation; TiO; $SrTiO_3$

Introduction

Transition metal oxides are viewed today as most promising materials in many fields, ranging from (photo)catalysis [1], through hydrogen production [2], resistive switching [3] and organic electronics [4],[5] to so-called thermoelectric power generators [6]. The performance of all of abovementioned applications is extremely sensitive to the work function (WF) of the active oxide layer. As a vast majority of applications is nowadays based on oxide heterostructures, not only macroscopic information of the work function is needed (which may be provided by averaging techniques like UPS) but also spatial resolution on the scale of single nanometers. Driven by its remarkable lateral and energetic resolution, Kelvin Probe Force Microscopy (KPFM, also known as Scanning Kelvin Probe Microscopy, SKPM) is a tool of choice for the precise measurements of WF across oxide heterostructures, which have not been fully exploited up to date. In recent years KPFM proved to be superior for many cases of both fundamental research and applications, like the identification of adsorption geometries of molecules on oxide surfaces [7], probing energetics of electron transfers within single molecules [8] and operation of prototypical electronic devices, like perovskite solar cells [9] or Ti/TiO_x/Ti memristive devices [10]. Out of two operation modes of KPFM, frequency modulation (FM) proves to be more suitable for investigation of oxide nanostructures, due to the higher lateral resolution than in amplitude modulation (AM) [11]. Therefore, in our study we present the advantages and limits of the FM-KPFM technique using the example of a newly discovered TiO/$SrTiO_3$(100) (metal/insulator) heterostructure, which have a potentially high technological relevance [12].

Now it would be justified to introduce both TiO and $SrTiO_3$ oxides, highlighting differences and similarities between those two structures. Judging on the electronic conduction, most transition metal oxides could be classified as insulators or semiconductors. However, due to the plenty of available valence states in which a cation can be, many transition metal oxides may also exhibit metallic conductivity. Here, a huge advantage over other materials is the possibility of oxides self-doping via introduction of oxygen vacancies [13], which is simultaneously a reason that there are not many reliable experimental studies on the work function of transition metal oxides [14]. $SrTiO_3$ is a perfect example of an insulator with a wide bandgap of 3.2 eV and also a model perovskite oxide. Ti^{4+} cations provide no electrons for the d-band, which can participate in conductivity. Strontium titanate finds many applications as dielectric ceramic material [15] but also in various heterostructures, e.g. in the search of exotic electron states (2DEG gas on the interface with $LaAlO_3$ [16], [17]). On the other side of the transition metal oxides spectrum lies titanium monoxide TiO, in which the titanium atoms adopt the valence state 2+, contributing to the formation of d^2 electrons. Hence, TiO is a d-band conductor, with a room temperature conductivity of 3500 Ω^{-1} cm^{-1}, slowly decreasing with temperature [18]. There is a growing interest in metallic oxides as reduced TiO nanostructures exhibit strong absorbance of light in a broad spectrum, which is of potential use in novel tumor therapy [19]. In the previous year many works were published on superconductivity of various TiO structures [20],[21]. According to those, rock-salt TiO is a type-II superconductor with superconductivity transition temperature

(T_c) of 5.5 K, which is higher than previously reported results [22]. Due to its interesting electronic structure, titanium monoxide nanoparticles find application in heterogeneous catalysis, e.g. for the hydrogenation of styrene [1].

Here we show the properties of a bulk-like crystalline rock-salt TiO phase, unlike previous studies on the crystallography and electronic structure of TiO, which were based on defective thin films formed on various surfaces e.g. TiC(100) [23] or TiO_2(110) [24]. γ-TiO is the high-temperature phase with a NaCl-type (rocksalt-type, B1) cubic structure (Fm3-m, a=4.184 Å), displaying a wide range of nonstoichiometry [25]. Our study contains first measurements of electrical conductivity and WF of crystalline TiO and its response to the ambient air re-oxidation. All above is compared to the work function of another relevant oxide $SrTiO_3$(100), showing similarities and differences between those two structures.

The presented manuscript is organized as follows: after the introduction of our TiO/$SrTiO_3$(100) system, a combined conductivity and work function study from the same surface area is presented, showing the possibility of obtaining full information on electronic properties, when KPFM is accompanied by conductive AFM. It is followed by the discussion of apparent variations of WF within cubic TiO nanowires, the estimation of the KPFM resolution and the differences between TiO_2 and SrO terminations of $SrTiO_3$(100). The last part of the study is dedicated to discuss the work function response of both TiO and $SrTiO_3$ surfaces upon oxidation via ambient air exposure, in order to provide an impression of oxygen, water and carbon dioxide interaction and also mimic operation conditions in real applications.

Results and Discussion

Thermal reduction of $SrTiO_3$(100) under reduced oxygen partial pressure (UHV conditions + an oxygen getter), assured by the ELOP (extremely low oxygen partial pressure) process, results in the formation of a network of ordered TiO nanowires on the (100) surface as shown in Fig. 1 a). Heavily reducing conditions enable not only the oxygen excorporation from the crystal but additionally trigger an incongruent sublimation of strontium, leaving the titanium enrichment of the surface [26]. This general process has been observed also for the broader class of transition metal oxides, such as $CaTiO_3$ or $BaTiO_3$. Titanium monoxide surface layer crystallizes in form of nanowires oriented along the main crystallographic directions of $SrTiO_3$(100), having a length of up to 10 µm, a width of a few hundred nm and a height of tens of nm. Their size could be easily tuned either by the temperature or time of reduction [12]. Perfect crystallographic order of TiO nanostructures is confirmed by the TEM measurements in the HAADF-STEM mode as we have recently shown in Ref. [12]. A closer look on TiO reveals the γ-TiO structure in a Fm-3m space group and 2.1 Å unit cell, which stands in agreement with literature values [27]. The high level of crystallinity of these nanowires is the result of the formation mechanism, which comprises incongruent strontium effusion from $SrTiO_3$ and then a TiO structure growth via crystallographic

shearing and diffusion (more details can be found in [12]). The abrupt TiO/$SrTiO_3$ interface and the Ti^{2+} to Ti^{4+} transition thereof makes such a transition metal oxide heterostructure a promising candidate for various electronic properties and charge transfer investigations.

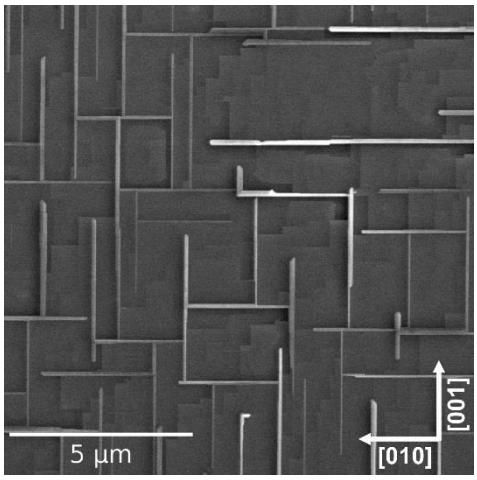

Fig. 1. SEM SE picture of an oriented network of titanium monoxide (TiO) nanowires on $SrTiO_3$(100). In-between terrace structure of STO could be seen.

Despite the similarities (both structures have cubic crystallographic phase), there are profound differences in the electronic structure between band insulator $SrTiO_3$ and metallic TiO. Here there are two 3d electrons per one Ti^{2+} divalent titanium ion, partially filling the metallic d-band in the energy diagram. From the orbital perspective, high conductivity is a consequence of the d-orbitals overlap from the neighbouring Ti sites. In the case of cubic TiO, the Ti-Ti distance is slightly above 2Å, which is enough to have a significant overlap given the d-orbitals extension. On the other hand, in the ideal $SrTiO_3$ perovskite there are no d-electrons on Ti sites. Thus a TiO network on $SrTiO_3$ constitutes a metallic nanowire array embedded in an insulator and to properly disentangle electronic properties of both structures a nanoscale resolving technique is needed. Indeed with the use of the LC-AFM technique the conductivity of the developed nanostructures at the nanoscale can be characterized providing a unique possibility of obtaining current maps as well as I/V characteristics at a given spot. Fig. 2a) and b) show topography and current maps of the TiO nanowire network on $SrTiO_3$(100). Apparently, TiO has a higher conductivity than the surrounding STO surface (areas at nanowires' rims of no current are due to technical reasons, such as wear of coating of the conductive probe). To better illustrate the differences, I/V characteristics of TiO and STO were collected and are presented in Fig. 2c). Given the apparent ohmic behavior at the TiO nanowire, the conductance of a whole system (tip + contact + TiO nanowire + interface + STO bulk + bottom electrode) could be estimated to G_{LCAFM} = 10 µS. In contrast, the STO surface exhibits one order of magnitude lower current of a rather semiconducting nature. It is noteworthy that the STO(100) surface had been beforehand thermally reduced up to 1150°C in UHV, resulting in the formation of a high concentration of

oxygen vacancies. Therefore the conductivity is much higher than that of a pristine crystal, which have been estimated via a comparable LC-AFM study to be around 10^{-16} S [28]. Here the observed changes of conductivity on the surface correlate directly with the work function differences as provided by the KPFM measurements taken at the very same area. It could be made possible by forcing the same conductive contact AFM tip to oscillate at higher harmonics to enter FM-KPFM mode (more details can be found here [29]). Fig. 2 d), e) present topography and work function of the same area. Differences in WF are as high as 900 meV between TiO and $SrTiO_3$, in favour of TiO, however there is also a certain variation within the TiO and $SrTiO_3$ structures, which will be discussed later. Bias sweep measurements presented in Fig. 2f) show reproducible Kelvin parabolae with negative curvature for both structures. As up and down bias sweeps appear to be the same, there is no sign of charging or charge transfer. A comparative study of LC-AFM and KPFM of $TiO/SrTiO_3$ structure enables a clear distinction between two materials of comparable conductivity but much different work functions. Although undoped $SrTiO_3(100)$ is a band insulator, it could be easily self-doped with oxygen vacancies upon thermal reduction [28], [30]. Reduction preferentially occurs at the surface, resulting in the reconstruction transformation from (1x1) to $(\sqrt{5}x\sqrt{5})R26.6°$, and in the vicinity of extended defects in a crystal (dislocations) which act as easy conduction paths for electrons. Oxygen vacancies formation and therefore Ti^{3+} valence, results in the appearance of new t_{2g} electron states within Ti 3d, below the conduction band of $SrTiO_3(100)$ [31]. Consequently a decrease of WF is expected, as it was previously reported for 900°C thermal annealing under UHV, where WF of $SrTiO_3(100)$ yielded 3.478(64) eV [30]. Hence, here a high conductivity of a reduced $SrTiO_3(100)$ is measured and a work function of 3.12(18) eV, which is almost 1 eV lower than previous XPEEM and UPS studies for untreated oxide – 4.13 and 4.2 eV [32], [33].

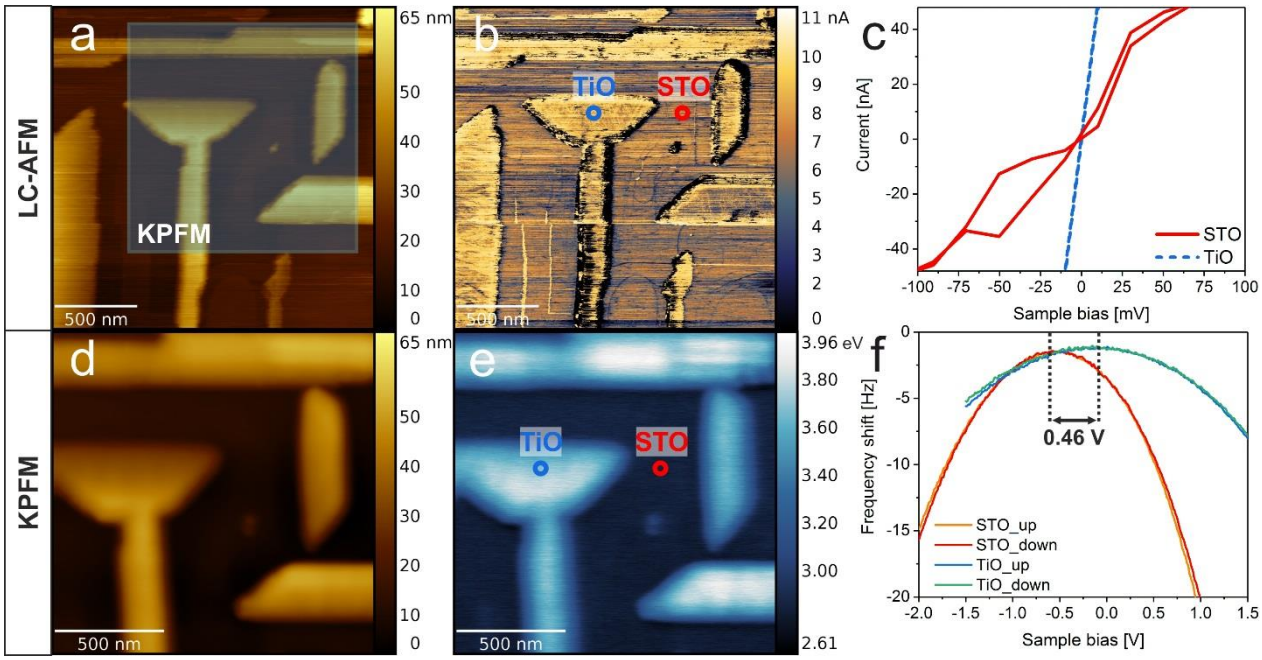

Fig. 2. Electrical properties of a TiO/$SrTiO_3$(100) heterostructures. a), b) LC-AFM topography and current (PtIr coated PPP-ContPt tip, +1 mV sample bias), c) I/V characteristic (up and down sweeps) of marked areas on TiO nanowire and STO surface, d), e) KPFM topography and work function measurement of the very same area, f) Kelvin parabolae at the same TiO and STO structures.

As stated before, KPFM investigations reveal certain variations in the work function value of TiO nanostructures. To illustrate this properly a 3D topography overprinted image with color scale representing the WF is shown in Fig. 3a). The WF of titanium monoxide varies as high as 300 meV, even within one nanowire. This is not an imaging artifact but rather a morphological-related feature, which is proved by the two profiles obtained for the same nanowire and shown in b) and c). Nanowires' edges have apparently different work function than a top surface. It is supposedly a consequence of different facets of a cubic TiO crystal exposed. Such an effect of facets having different WF was to date observed for many structures – differences could be as high as 255 meV measured for the case of (-1-1-2) and (110) surfaces of $CuGaSe_2$ [34]. For the case of transition metal oxide crystals XPEEM studies proved that the WF of the $SrTiO_3$(111) face is higher than that of the (100) face by no less than 210 meV [32]. Smaller differences in the range of 70 meV were reported for the case of titanium dioxide (110) and (100) faces [35]. In the present case the differences could be higher due to the fact that whole sample with TiO nanostructures were annealed up to 1150°C and thus a possible reduction-driven non-stoichiometry occurs. From a geometrical perspective low index faces of cubic TiO, like (100), (110) or (210) have an equal number of protruding oxygen and titanium atoms, in contrary to the (111) face, where a whole plane is formed by either titanium or oxygen. Up to our knowledge there are no literature studies on the stability or work function on such faces but it is justified to assume certain differences between those facets, which are also influenced by the preferential removal of oxygen during thermal reduction. As TiO nanowires have a height of tens of nm and tip convolution may play a role, a precise evaluation of steep facets of a higher WF seen in Fig. 3 is difficult. Basing on the relative slope of a TiO surface it seems that the top adopts typically (100) plane but it needs further proofs.

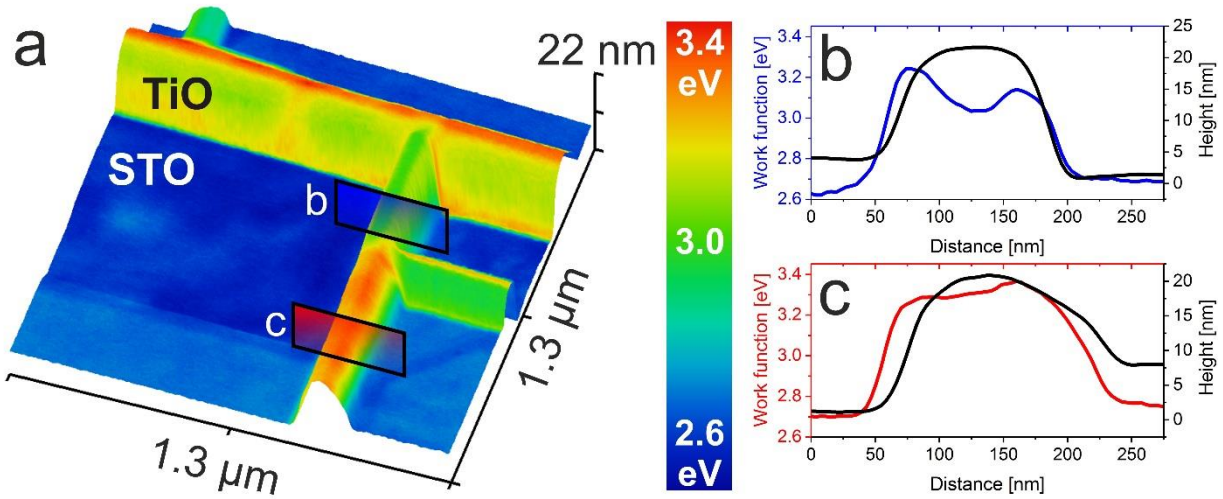

Fig. 3. TiO facets influence on the nanoscale work function. a) 3D view of the combined topography and WF of TiO/$SrTiO_3$. b), c) topography and work function profiles of two areas on the same TiO nanowire.

An overlayer of work function on topography shown in Fig. 3a) provides additional information on the high lateral contrast of KPFM. WF and morphology matches almost completely, although height variations are of tens of nm. To investigate the resolution limits of the KPFM imaging of oxide heterostructures with a complex topography a set of images of parallel TiO nanowires was investigated and the results are presented in Fig. 4. As a measure of the potential resolution we have used the ratio between the CPD decrease in-between the TiO nanowires and the full CPD of TiO with respect to STO. For an ideal case, when the CPD reaches the value of STO in the gap between parallel nanowires, this measure adopts 1, and 0 if there is no drop in CPD. The dependence of this value on TiO nanowires separation, plotted in Fig. 4 d) provides information on the resolution limit. Apparently it follows an asymptotic behavior and the correct CPD values are measured when TiO nanowires are separated by more than 40 nm. This stands in a perfect agreement with the real tip radius of 15 nm, which was measured for the same cantilever in HR-SEM (see Fig. 4d) insets). Here, the use of uniformly PtIr-coated tips, enables avoidance of the topography correlated artifacts, unlike some previous studies [36]. Taking into account the opening angle of about 40 degrees and the nanowires' average height of 18(8) nm, the tip diameter at the level of nanowires top surface would be about 40 nm, meaning that the CPD resolution is approaching the topography resolution which is the ultimate physical limit of FM-KPFM technique [11]. Similar results were obtained for the resolution estimation for KBr nanoislands of monoatomic thickness, where a resolution of 0.5 was obtained for 20 nm separation, as it is in following study [37]. CPD resolution at TiO/$SrTiO_3$ transition is insensitive to nanowires' height, following the same asymptotic behavior (see Fig. 4 d), unlike the situation for C60 islands on HOPG, where spread of 50 nm was reported, while topography resolution yielded 10 nm [38].

From our results we can set the limit of the smallest separation of oxide nanostructures at 15 nm to obtain any CPD difference. As for the CPD resolution, the estimated value would be below 5 meV, due to the high mechanical stability and good conductivity of both platinum silicide and PtIr-coated tips.

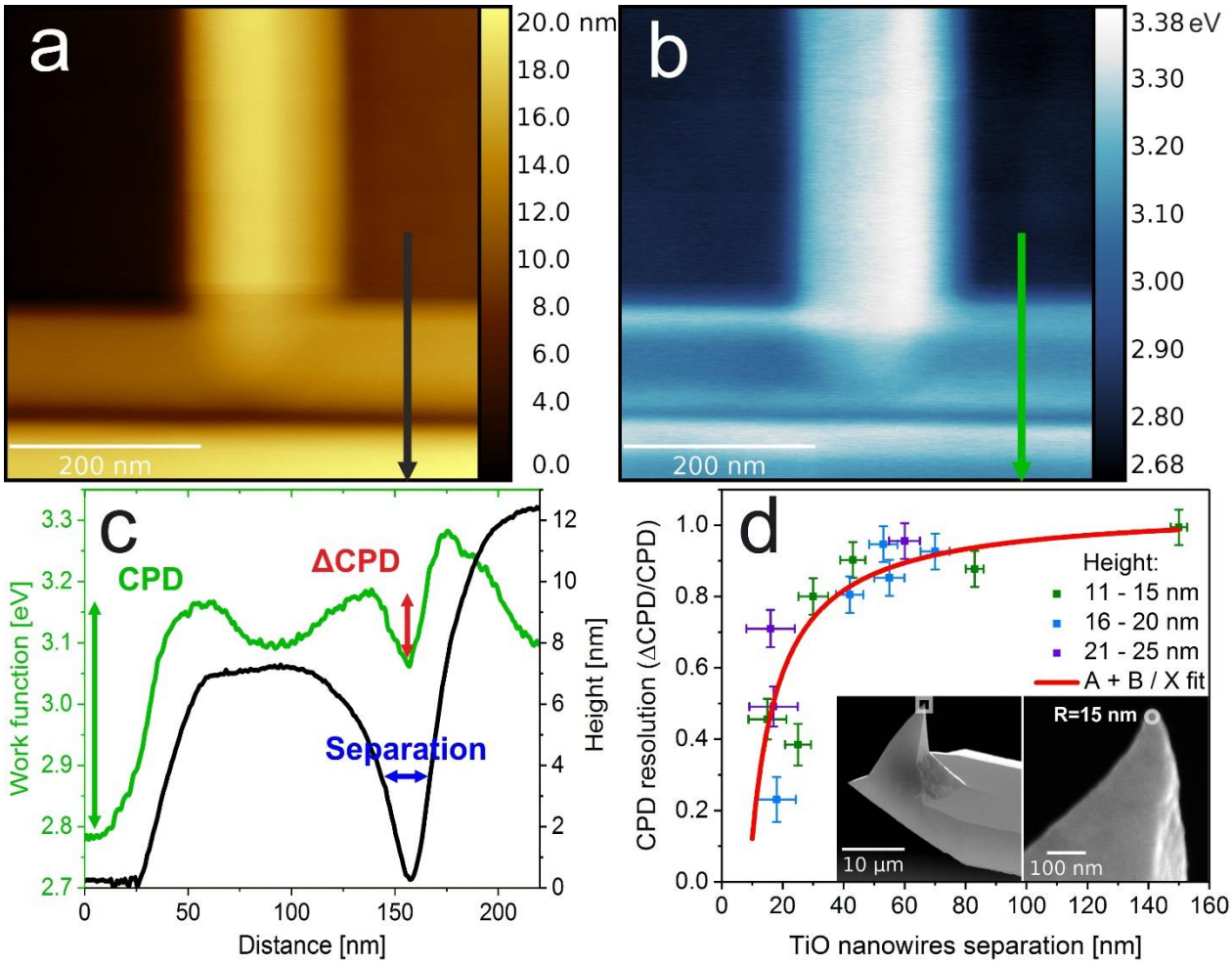

Fig. 4. KPFM lateral resolution on high TiO/STO structures. a) Topography and b) Work function of TiO nanowire array on $SrTiO_3$(100), c) Height (black line) and work function (green line) profiles of two adjacent TiO nanowires, showing high KPFM contrast, d) Dependence of the CPD resolution (estimated as ΔCPD/CPD, see c)) on separation between TiO nanowires, with A + B/X asymptote fit. Insets show SEM images of the actual PtSi cantilever used in the experiments with a tip radius of 15 nm.

Apart from the work function difference between the TiO and STO materials we have found also that the CPD/WF mapping of the STO(100) itself exhibits a nonuniform nature. This has been associated with two different possible surfaces, as $SrTiO_3$(100) perovskite structure has two stable non-polar terminations: SrO and TiO_2, which both are present on the pristine surface, although TiO_2 being more stable [39]. When annealed under reducing conditions, the TiO_2 termination is promoted. Upon heavy reduction there is a further oxygen depletion which results in the formation of the $(\sqrt{5}x\sqrt{5})R26.6°$ reconstruction, which we recently proved to be Ti-enriched layer on TiO_2 terminated $SrTiO_3$(100) [30], [40]. The electronic structures of both terminations are much different – DFT calculated work function values are 1.92 eV and 4.48 eV for SrO and TiO_2 respectively [14], obtained however for the pure surfaces, without vacancies.

In the present case of thermally reduced $SrTiO_3$(100), the majority of surface adopts $(\sqrt{5}x\sqrt{5})R26.6°$ reconstruction on TiO_2 termination, as shown in the inset in Fig. 5a). Bright features seen in the STM picture are either oxygen vacancies/vacancy clusters or Sr adatoms,

according to the model [30]. KPFM reveals a non-homogeneous landscape of work function - higher values are measured on terraces, whereas areas near edges have reduced work function (see Fig. 5b). It could be directly represented by the histogram shown in Fig. 5c). A clear difference of 23 meV could be measured between two areas. Supposedly the higher values are related to the TiO_2 termination, which is dominant and lower to SrO-enriched terrace edges. This assignment is supported by the measured KPFM difference of air-annealed $SrTiO_3$ terminations of approx. 10 meV [41]. This difference is not likely to be caused by the electronic depleted layer at step edges, since it stretches out from the edges up to 100 nm, which is too far to be attributed to local dipoles.

In terms of absolute work function of TiO_2-terminated $SrTiO_3$(100), the obtained value of 3.12(18) eV, averaged across a number of images, is close to those postulated by the DFT for TiO_2 termination with oxygen vacancies in the surface layer – 3.39 eV [14]. On the other hand, the measured values at SrO-rich terrace edges are higher compared to the reported value of 2.5-3.0 eV for single terminated $SrTiO_3$(100) [42]. It is most likely a result of high defective state of those regions, which are thought to be more unstable and reactive compared to TiO_2-termination [42].

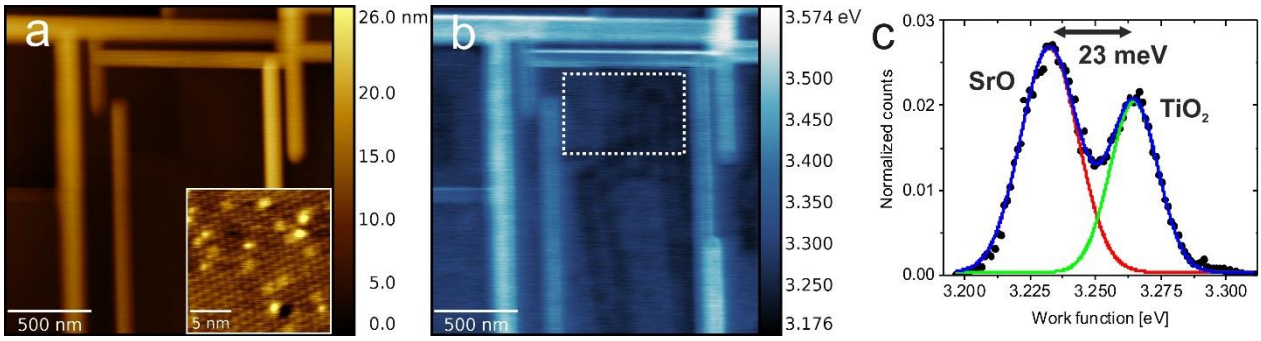

Fig. 5. Identification of the $SrTiO_3$ termination via KPFM. a) Topography of a TiO/$SrTiO_3$ structure (Δf = -20 Hz); inset shows the TiO_2-based (√5x√5)R26.6° reconstruction (STM empty states, +1.5V, 10 pA), b) Corresponding work function map from KPFM, c) Work function histogram from the selected area in b).

Ambient air re-oxidation of TiO and $SrTiO_3$

As a vast majority of applications of transition metal oxides is related to the oxygen activity and redox reactions on surfaces, the next experiment was aimed to study the work function dependence upon controlled re-oxidation of reduced oxides.

Transition metal oxide nanostructures find manifold applications especially in various (photo)catalytic processes, e.g. water splitting [1][43][44]. For industrial uses samples have to be exposed to ambient conditions, therefore it is necessary to investigate impact of an air exposure on electronic surface properties. Moreover, transition metal oxides are often regarded as promising materials for sensing applications, due to the strong response to gaseous pressures, especially oxygen and water [45]. A tool of choice, which provides information of subtle changes in the work function is KPFM, which has been used to date for research on the photocatalytic

activity of TiO_2-based doped and undoped nanofibers [46], [47] and for the understanding the operation of nanostructure electrochemical sensors [48].

Thus, we focused on the systematic approach of the influence of ambient air on the work function of TiO and $SrTiO_3$(100). Fig. 7a) shows topography and work function of representative TiO nanowire networks before and after ambient air exposure. Additionally, the impact of low temperature annealing (230°C) in UHV is presented. After venting of the vacuum chamber, the TiO nanowires still had a much higher work function than the $SrTiO_3$(100) surface, however the absolute values for both materials rose. It is widely known that water molecules present in the ambient air form a dipole layer, which can give rise to the effective surface potential [49].

To reduce the impact of weakly-interacting physisorbates, in the next step the sample underwent *in situ* UHV annealing, which implicated in WF decrease of both TiO and $SrTiO_3$ by about 0.3 eV. This is regarded as a limit value of physisorbed adsorbates binding energy. To illustrate the experimental findings better, three histograms of reduced, air oxidized and outgased work functions are plotted in Fig. 7b). It is immediately visible that the general three-peak nature of STO, lower and higher TiO values of WF is preserved, however the offset changes, as illustrated in Fig. 7c). STO(100) work function increases by 0.9 eV due to the air exposure, similarly as for the case of oxygen re-oxidation [30]. A conclusion can be drawn that the most active gas is oxygen which refills vacancies of the reduced $(\sqrt{5}x\sqrt{5})R26.6°$ surface and locally oxidizes titanium cations to regain 4+ valence state.

Vented TiO nanowires have a work function higher by 0.65 eV, independent on face, which is almost 0.5 eV higher than for the case of pure oxygen (not shown). It is a footprint of the high catalytic activity of TiO surface, which was previously postulated for the case of TiO/TiO_2 nanoparticles [44]. Reduced titania $TiO_{1.23}$ proves to be a promising candidate for electrochemical water splitting [50]. As catalytic activity of a crystalline rock-salt TiO phase has not been yet studied, this is a first indirect observation of a high potential of such structure.

After *in situ* annealing to 230°C, the work function of TiO nanowires drops by 0.2 eV, in contrary to a 0.35 eV decrease for $SrTiO_3$(100) surface. A temperature of 230°C was chosen to enable desorption of physisorbed adsorbates, leaving however chemisorbed species. Numerical calculations suggests that H_2O and CO_2 species in air saturate almost all free adsorption sites on TiO_2-terminated $SrTiO_3$(100) [51]. The low Redhead desorption temperatures of H_2O (CO_2) of 233–283 K (428–523 K) calculated by Baniecki et al. [51] suggest that our surface, which is predominantly TiO_2-terminated is cleaned of those adsorbates after annealing, hence the 0.35 eV difference in WF.

The lower response of TiO to annealing is a hint of higher adsorption energy of interacting gases. It suggests chemisorption of H_2O and CO_2 and of their dissociation products, stemming from profound catalytic activity of TiO phase.

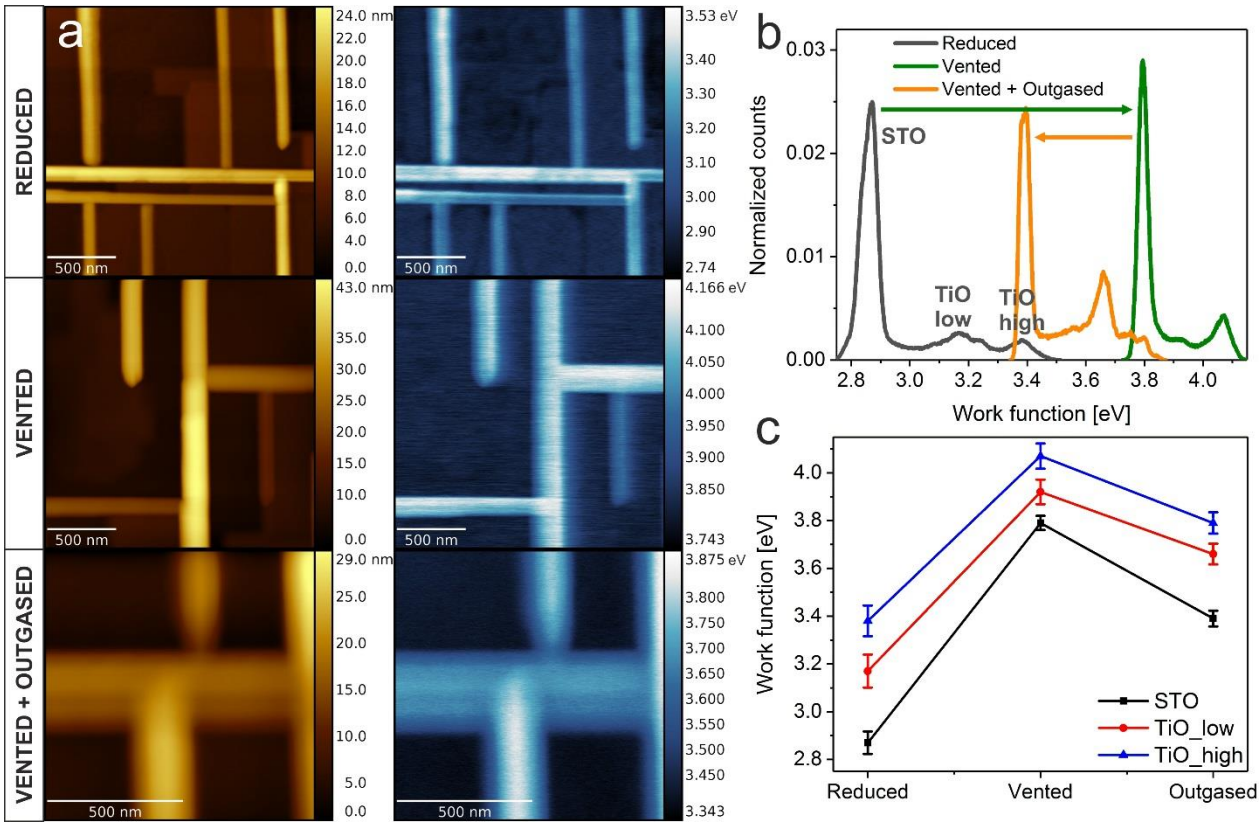

Fig. 6. Influence of the air exposure on TiO/$SrTiO_3$ work function. a) KPFM topography and work function of TiO/$SrTiO_3$ heterostructure (Δf = -40 Hz) after reduction (first row), exposed to ambient air (second row) and after annealing up to 230°C (third row). b) Work function histograms of presented cases. c) Evolution of the work function value for $SrTiO_3$(100) surface (black), lower TiO facets (red) and higher (blue).

To wrap up our experimental findings of the KPFM study of TiO and $SrTiO_3$(100) crystals a comparison between obtained work functions as well as literature values is presented in Table 1. The first direct work function measurement of cubic γ-phase of TiO yields 3.31(21) eV for the as-grown (reduced in UHV at 1150°C) and 3.75(11) eV for vented and outgased, which is most likely close to the value for pristine TiO crystal. Up to date only values for TiO WF are coming from polycrystalline samples (films, nanoparticles) and from laterally averaging method of UPS, thus it cannot be reasonably compared with our findings. WF value obtained for the reduced $SrTiO_3$(100) surface – 3.12(18) eV follows the trend of decreasing work function upon reduction and increasing due to re-oxidation [30]. It is worth mentioning that substantial discrepancies between measured WF for transition metal oxides, besides different quality of samples, could stem from the non-optimal conditions during preparation, e.g. holder materials can act as oxygen getters, influencing the reduction state of a sample [12].

Material	Sample	WF [eV]	Method	Reference
TiO	TiO nanoparticles (14 nm)	3.01	UPS	[44]
	TiO thin polycrystalline film	~ 4.5	UPS	[52]
	TiO cubic γ-phase (nanowires): • Reduced • Air-exposed • Air-exposed and annealed	 3.31(21) 3.92(17) 3.75(11)	KPFM	**This study**
$SrTiO_3$	$SrTiO_3$(100) $SrTiO_3$(110) $SrTiO_3$(111)	4.13 4.32 4.34	XPEEM	[32]
	$SrTiO_3$(100)	4.2	UPS	[33]
	$SrTiO_3$(100) reduced at 900°C	3.478(64)	KPFM	[30]
	TiO_2-terminated $SrTiO_3$(100) SrO-terminated $SrTiO_3$(100)	4.2 – 4.3 2.5 – 3.0	Macroscopic Kelvin probe	[42]
	$SrTiO_3$(100) (single crystal): • Reduced at 1150°C • Air-exposed • Air-exposed and annealed	 3.12(18) 3.835(72) 3.41(11)	KPFM	**This study**
	$SrTiO_3$(100) BHF etched, air annealed (1000°C) • ϕ_{TiO2} - ϕ_{SrO} difference	 ~10 meV	KPFM	[41]
	$SrTiO_3$(100) reduced in UHV at 1150°C • ϕ_{TiO2} - ϕ_{SrO} difference	 23(5) meV	KPFM	**This study**

Table 1. Comparison between literature values and obtained experimental results of TiO and $SrTiO_3$ work functions.

Conclusions

We have presented a thorough study of the Kelvin Probe Force Microscopy investigations on electronic properties of a cubic TiO formed on $SrTiO_3$(100) single crystal surface. To our best knowledge, this is the first measurement of the crystalline TiO work function and its dependence on a gaseous pressure of air, in comparison to $SrTiO_3$(100) response. The rock-salt cubic γ-phase, with a high crystallographic order, has a work function of 3.31(21) eV with significant variations on the surface, which are supposedly related to different facets exposed. Higher work function of TiO compared to STO(100) is accompanied with higher conductivity, with an Ohmic behavior, which was checked by simultaneous LC-AFM measurements. Full ambient venting results in a 0.6 eV rise in the TiO work function, being a hint of ongoing catalyzed dissociation of CO_2 and H_2O present in ambient air. The work function of TiO decreases by 0.2 eV as a result of 230°C UHV annealing, being a measure of amounts of physisorbed species. Air exposure of $(\sqrt{5}x\sqrt{5})R26.6°$ TiO_2-terminated $SrTiO_3$(100) surface results in 0.9 eV increase in work function, which is similar to the rise for the re-oxidation in pure oxygen. Annealing causes decreases of 0.4 eV due to the desorption of weakly bonded CO_2 and H_2O species.

Our study contains also an estimation of the KPFM lateral resolution, which supposedly enabled for reliable measurements of TiO nanowires separated by 40 nm, proving suitability of the KPFM

technique for transition metal oxide structures investigation, even with remarkable topographical variations.

Concluding, our results acquired for crystalline TiO and $SrTiO_3$ phases give an important information of the work function values itself but also on the oxygen and air interaction, towards development of reliable transition metal oxide catalytic and sensing devices.

Experimental

We investigated Verneuil-grown epi-polished $SrTiO_3$(100) crystals, provided by the Crystec company. Crystals were mounted onto Omicron direct heating holders and introduced into the UHV chamber, with a base pressure of 5×10^{-10} mbar, maintained by use of turbomolecular, ion and sublimation pumps. In order to produce a TiO nanowires network on the surface of STO(100) the Extremely Low Oxygen Partial Pressure (ELOP) method of perovskite decomposition was adapted (for more information see [26],[12]). The $SrTiO_3$(100) single crystal ($10\times3\times0.5$ mm^3) sample was mounted on a n-doped Si(111) single crystal, which acted as an oxygen getter, allowing for reaching the extremely low effective oxygen partial pressures on the STO surface (below 10^{-20} mbar). As a result of high-temperature reduction (1150°C, 1h) under such conditions, a macroscopic network of nanowires was formed. After slow cooling down to room temperature, samples were transferred *in situ* to the microscope chamber of an Omicron RT STM/AFM system, where Kelvin Probe Force Microscopy (KPFM), Local-conductivity Atomic Force Microscopy (LC-AFM) and Scanning Tunneling Microscopy (STM) measurements were performed. The KPFM operating in FM mode was used with a single-pass method, with three feedback loops maintaining oscillation amplitude, phase and frequency shift [53]. The real oscillation amplitude was in the range of 10 nm. In order to obtain the CPD signal an AC modulated bias was applied to the bottom electrode, where a sample was mounted. The modulation frequency and amplitude was set to 315 Hz and 500 mV, respectively.

In order to ensure reproducible FM-KPFM results two different types of AFM cantilevers were used: PPP-ContPt (PtIr coated) and PtSi-FM (platinum silicide tips), both from Nanosensors. Such cantilevers are widely used as conducting tips in a contact mode AFM, allowing for a high lateral resolution in conductivity measurements. Remarkable mechanical stability of selected cantilevers allowed for the non-contact mode measurements (with a Kelvin loop) using the very same tip, maintaining oscillations at the higher harmonics of the fundamental frequency (approx. 75 kHz). Hence, in order to record current and CPD maps from the very same sample area, at first KPFM measurements were performed, with the soft cantilever forced to oscillate at higher harmonics, then tip was retracted tens of nm from the surface, all feedback loops were turned down and a contact mode AFM scan was performed when approached, with a single loop maintaining deflection setpoint of 10-30 mV. High conductivity of both TiO and STO materials enabled for use of low sample bias of +1 mV for the LC-AFM measurements.

Real work function values were calculated from recorded CPD maps after calibration against material of a known work function, here highly oriented pyrolytic graphite (HOPG), annealed *in situ* up to 300°C, in order to remove water and other physisorbates. After each set of KPFM measurements a HOPG surface was scanned, using the same experimental parameters and a V_{CPD}(HOPG) was obtained. Assuming HOPG work function of ϕ_{HOPG} = 4.5 eV (literature values: 4.6 ± 0.1 eV [54], 4.4 ± 0.1 eV [55]), work function of TiO/STO was evaluated using formula: $\phi_{TiO/STO} = V_{CPD}(TiO/STO) - V_{CPD}(HOPG) + \phi_{HOPG}$.

Ambient air exposure was realized by venting the sample in the load-lock and then introducing again into UHV system. Subsequent annealing up to 230°C for 1h hour enabled for the estimation of physisorbed species' content at the surface.

Acknowledgements

Support by the Polish National Science Center (UMO- 2018/29/B/ST5/01406) is acknowledged

References

[1] Imran, M., Yousaf, A. B., Zhou, X., Jiang, Y. F., Yuan, C. Z., Zeb, A., ... & Xu, A. W. (2017). Pd/TiO Nanocatalyst with Strong Metal–Support Interaction for Highly Efficient Durable Heterogeneous Hydrogenation. The Journal of Physical Chemistry C, 121(2), 1162-1170.

[2] Compton, Richard G., ed. Electrode kinetics: reactions. Vol. 27. Elsevier, 1987.

[3] Waser, Rainer, et al. "Redox-based resistive switching memories–nanoionic mechanisms, prospects, and challenges." Advanced materials 21.25-26 (2009): 2632-2663.

[4] Yu, Xinge, Tobin J. Marks, and Antonio Facchetti. "Metal oxides for optoelectronic applications." Nature materials 15.4 (2016): 383.

[5] Wrana, Dominik, et al. "Growth of para-Hexaphenyl Thin Films on Flat, Atomically Clean versus Air-Passivated TiO2 (110) Surfaces." The Journal of Physical Chemistry C 119.29 (2015): 17004-17015.

[6] Lin, Yue, et al. "Thermoelectric power generation from lanthanum strontium titanium oxide at room temperature through the addition of graphene." ACS applied materials & interfaces 7.29 (2015): 15898-15908.

[7] Jöhr, Res, et al. "Characterization of individual molecular adsorption geometries by atomic force microscopy: Cu-TCPP on rutile TiO2 (110)." The Journal of chemical physics 143.9 (2015): 094202.

[8] Fatayer, Shadi, et al. "Reorganization energy upon charging a single molecule on an insulator measured by atomic force microscopy." Nature nanotechnology 13.5 (2018): 376.

[9] Axt, Amelie, et al. "Know your full potential: Quantitative Kelvin probe force microscopy on nanoscale electrical devices." Beilstein journal of nanotechnology 9.1 (2018): 1809-1819.

[10] Batko, I., and M. Batkova. "AFM-utilizing approach to search for new oxide materials for perspective applications in memristive devices." The European Physical Journal-Applied Physics 58.2 (2012).

[11] Zerweck, Ulrich, et al. "Accuracy and resolution limits of Kelvin probe force microscopy." Physical Review B 71.12 (2005): 125424.

[12] Wrana, Dominik, et al. "A bottom-up process of self-formation of highly conductive titanium oxide (TiO) nanowires on reduced SrTiO 3." Nanoscale 11.1 (2019): 89-97.

[13] Su, J., Zou, X., & Chen, J. S. (2014). Self-modification of titanium dioxide materials by Ti 3+ and/or oxygen vacancies: new insights into defect chemistry of metal oxides. Rsc Advances, 4(27), 13979-13988.

[14] Zhong, Zhicheng, and Philipp Hansmann. "Tuning the work function in transition metal oxides and their heterostructures." Physical Review B 93.23 (2016): 235116.

[15] Zhang, Tian-Fu, et al. "High-Temperature Dielectric Relaxation Behaviors of Relaxer-Like PbZrO3–SrTiO3 Ceramics for Energy-Storage Applications." Energy Technology 4.5 (2016): 633-640.

[16] Ohtomo, A., and H. Y. Hwang. "A high-mobility electron gas at the LaAlO 3/SrTiO 3 heterointerface." Nature 427.6973 (2004): 423.

[17] Song, Qi, et al. "Observation of inverse Edelstein effect in Rashba-split 2DEG between SrTiO3 and LaAlO3 at room temperature." Science advances 3.3 (2017): e1602312.

[18] Yamashita, Jiro. "Electronic Structure of TiO and NiO." Journal of the Physical Society of Japan 18.7 (1963): 1010-1016.

[19] Shu, G., Wang, H., & Zhang, X. (2018). Microwave-Assisted Synthesis of Black Titanium Monoxide for Synergistic Tumor Phototherapy. ACS applied materials & interfaces.

[20] Xu, Jijian, et al. "Nano Titanium Monoxide Crystals and Unusual Superconductivity at 11 K." Advanced Materials 30.10 (2018): 1706240.

[21] Zhang, C., Hao, F., Gao, G., Liu, X., Ma, C., Lin, Y., ... & Li, X. (2017). Enhanced superconductivity in TiO epitaxial thin films. npj Quantum Materials, 2(1), 2.

[22] Wang, D., Huang, C., He, J., Che, X., Zhang, H., & Huang, F. (2017). Enhanced Superconductivity in Rock-Salt TiO. ACS Omega, 2(3), 1036-1039.

[23] Shirotori, Y., et al. "Electronic structure and reactivity of the TiO thin film formed on a TiC (100) surface." Thin solid films 464 (2004): 76-79.

[24] Pabón, B. M., Beltrán, J. I., Sánchez-Santolino, G., Palacio, I., López-Sánchez, J., Rubio-Zuazo, J., ... & Varela, M. (2015). Formation of titanium monoxide (001) single-crystalline thin film induced by ion bombardment of titanium dioxide (110). *Nature communications*, *6*, 6147.

[25] Amano, S., Bogdanovski, D., Yamane, H., Terauchi, M., & Dronskowski, R. (2016). ε-TiO, a Novel Stable Polymorph of Titanium Monoxide. Angewandte Chemie International Edition, 55(5), 1652-1657.

[26] Rodenbücher, Christian, et al. "Stability and Decomposition of Perovskite-Type Titanates upon High-Temperature Reduction." physica status solidi (RRL)–Rapid Research Letters 11.9 (2017): 1700222.

[27] M. D. Banus, T. B. Reed, A. J. Strauss, Phys. Rev. B 1972, 5, 2775-2784.

[28] Szot, Krzysztof, Gustav Bihlmayer, and Wolfgang Speier. "Nature of the Resistive Switching Phenomena in TiO2 and SrTiO3: Origin of the Reversible Insulator–Metal Transition." Solid State Physics. Vol. 65. Academic Press, 2014. 353-559.

[29] Rodenbücher, C., et al. "Electrical nanopatterning of TiO2 single crystal surfaces in situ via local resistance and potential switching." APL Materials 6.6 (2018): 066105.

[30] Wrana, Dominik, et al. "In situ study of redox processes on the surface of SrTiO3 single crystals." Applied Surface Science 432 (2018): 46-52.

[31] Zhong, Zhicheng, and Paul J. Kelly. "Electronic-structure–induced reconstruction and magnetic ordering at the LaAlO3| SrTiO3 interface." EPL (Europhysics Letters) 84.2 (2008): 27001.

[32] Zagonel, Luiz Fernando, et al. "Orientation-dependent work function of in situ annealed strontium titanate." Journal of Physics: Condensed Matter 21.31 (2009): 314013.

[33] Chung, Yip-Wah, and W. B. Weissbard. "Surface spectroscopy studies of the SrTi O 3 (100) surface and the platinum-SrTi O 3 (100) interface." Physical Review B 20.8 (1979): 3456.

[34] Sadewasser, S., et al. "High-resolution work function imaging of single grains of semiconductor surfaces." Applied Physics Letters 80.16 (2002): 2979-2981.

[35] Imanishi, Akihito, Etsushi Tsuji, and Yoshihiro Nakato. "Dependence of the work function of TiO2 (Rutile) on crystal faces, studied by a scanning auger microprobe." The Journal of Physical Chemistry C 111.5 (2007): 2128-2132.

[36] Polak, Leo, and Rinke J. Wijngaarden. "Preventing probe induced topography correlated artifacts in Kelvin Probe Force Microscopy." Ultramicroscopy 171 (2016): 158-165.

[37] Krok, F., et al. "Lateral resolution and potential sensitivity in Kelvin probe force microscopy: Towards understanding of the sub-nanometer resolution." Physical Review B 77.23 (2008): 235427.

[38] Sadewasser, S., et al. "The influence of surface topography on Kelvin probe force microscopy." Nanotechnology 20.50 (2009): 505503.

[39] Jang, Yun Hyeong, and Jin Hyung Cho. "Surface potential distribution of a LaAlO3 film on mixed termination SrTiO3." Journal of the Korean Physical Society 69.5 (2016): 783-788.

[40] Martirez, John Mark P., et al. "Atomic and Electronic Structure of the BaTiO 3 (001)(5× 5) R 26.6° Surface Reconstruction." Physical review letters 109.25 (2012): 256802.

[41] Gellé, Florian, et al. "Guideline to atomically flat TiO 2-terminated SrTiO 3 (001) surfaces." Surface Science (2018).

[42] Susaki, Tomofumi, Asahi Makishima, and Hideo Hosono. "Work function engineering via LaAlO 3/SrTiO 3 polar interfaces." Physical Review B 84.11 (2011): 115456.

[43] Muuronen, Mikko, et al. "Mechanism of photocatalytic water oxidation on small TiO 2 nanoparticles." Chemical science 8.3 (2017): 2179-2183.

[44] Chen, Zhenrui, et al. "Photocatalytic activity enhancement of anatase TiO2 by using TiO." Journal of Nanomaterials 2014 (2014).

[45] Henning, A., Günzburger, G., Jöhr, R., Rosenwaks, Y., Bozic-Weber, B., Housecroft, C. E., ... & Glatzel, T. (2013). Kelvin probe force microscopy of nanocrystalline TiO2 photoelectrodes. Beilstein journal of nanotechnology, 4, 418.

[46] Wu, Ming-Chung, et al. "Photo-Kelvin probe force microscopy for photocatalytic performance characterization of single filament of TiO 2 nanofiber photocatalysts." Journal of Materials Chemistry A 1.18 (2013): 5715-5720.

[47] Wu, Ming-Chung, et al. "Photocatalytic activity of nitrogen-doped TiO 2-based nanowires: a photo-assisted Kelvin probe force microscopy study." Journal of nanoparticle research 16.1 (2014): 2143.

[48] Henning, Alex, and Yossi Rosenwaks. "KPFM of Nanostructured Electrochemical Sensors." Kelvin Probe Force Microscopy. Springer, Cham, 2018. 367-389.

[49] Kim, Haeri, and Dong-Wook Kim. "Transport characteristics and surface potential distribution of electrically stressed TiO 2 single crystals." Applied Physics A 102.4 (2011): 949-953.

[50] Swaminathan, Jayashree, Ravichandran Subbiah, and Vengatesan Singaram. "Defect-Rich Metallic Titania (TiO1. 23) An Efficient Hydrogen Evolution Catalyst for Electrochemical Water Splitting." ACS Catalysis 6.4 (2016): 2222-2229.

[51] Baniecki, J. D., et al. "Chemisorption of water and carbon dioxide on nanostructured BaTiO 3–SrTiO 3 (001) surfaces." Journal of Applied Physics 106.5 (2009): 054109.

[52] Greiner, Mark T., et al. "Transition metal oxide work functions: the influence of cation oxidation state and oxygen vacancies." Advanced Functional Materials 22.21 (2012): 4557-4568.

[53] F. Krok, J.J. Kolodziej, B. Such, P. Czuba, P. Struski, P. Piatkowski, M. Szymonski. Surface Science 566–568 (2004) 63–67.

[54] Melitz, Wilhelm, et al. "Scanning tunneling spectroscopy and Kelvin probe force microscopy investigation of Fermi energy level pinning mechanism on InAs and InGaAs clean surfaces." Journal of Applied Physics 108.2 (2010): 023711.

[55] Jeong, Hae Kyung, et al. "Valence band of graphite oxide." EPL (Europhysics Letters) 92.3 (2010): 37005.